Dynamic Infrared Imaging Simulation of Small Aerial Target

Jiahao Wang and Jun Yang

September 23, 2021

Dynamic infrared imaging simulation of small aerial target

Jiahao Wang
School of Automation
Northwestern Polytechnical University
Xi'an China
wjh857391372@163.com

Jun Yang
School of Automation
Northwestern Polytechnical University
Xi'an China
junyang@nwpu.edu.cn

***Abstract*—Infrared imaging simulation has great application potentials in both military and civil fields and is widely used in target detection and recognition, sensor performance evaluation, military training and so on. This paper presents a dynamic infrared imaging simulation method of small aerial target. The infrared radiation model of the target, including spontaneous radiation model and reflection model, is studied. The generalized Gaussian model is used to simplify the gray distribution model of the target. The optical and electronic models of infrared sensors are studied, and the gray mapping of the model is used to get the maximum gray value of the target, considering the transmittance of atmospheric transmission. Background is initialized using any infrared sky image and then adjusted the visibility by the camera perspective model. Then simulated target is fused with the simulated background using Poisson fusion for the generation of a more natural image. A dynamic simulation is fulfilled by assuming kinetics models of the target and the observer. Experimental results show that the proposed system works in real time and the simulated images are very similar to the real infrared images.**

Keywords—infrared imaging, simulation, small aerial target, background, Poisson fusion

I. INTRODUCTION

Infrared imaging of aerial targets, especially the early detection and tracking of distant aerial targets, is one of key technologies for aircraft navigation, missile guidance and air surveillance[1]. However, running flight tests for a newly developed infrared system are usually time consuming and cost expensive, sometimes even impossible for certain testing scenarios. Infrared imaging simulation of aerial targets is an effective solution and is in an urgent need in many fields. Ideally, a simulation system can test as many different scenarios as it can in a very low cost and high efficiency, e.g. various parameter settings, different weather conditions and dynamic encountering situation between aircrafts.

Several studies have done research on the infrared simulation of small aerial targets. Zhong [2] generates the infrared small target by manually setting the scale and gray distribution, and then fuses the small target with the static background to obtain the infrared simulation images of small target under complex background. The simulation process does not consider the factors that affect the small aerial target imaging, and the background is static, the simulation scene is limited. Wang [3] studies the process of aerial target imaging, but only simulates the target without fuse it with the background, which is relatively limited in practical application.

In this paper, we propose an infrared imaging simulation system of aerial targets. Since it is significant to detect distant aerial targets, which will only occupy a few pixels in the image, we focus on simulation of small aerial targets. With a simplified 3D targe model, the major concerns for target simulation is the modelling of self-radiation and reflection radiation, as well as the atmospheric transfer effect. Background is initialized using any infrared sky image and then adjusted the visibility by the camera perspective model. Then simulated target is fused with the simulated background using Poisson fusion for the generation of a more natural image. A dynamic simulation is fulfilled by assuming kinetics models of the target and the observer. So different encountering situation between the target and the observer can be simulated easily. Our main contribution is the designing of a flexible infrared imaging simulation system, which is capable of simulate various scenarios in a high efficiency.

II. RELATED WORK

A. Thermal infrared modeling

For thermal infrared modeling, physics-based model and empirical model can be used. PRISM (Physically Reasonable Infrared Signature Model) has been a surface temperature field prediction model based on the first law of thermodynamics. Parameters of object material, surrounding environment and atmospheric condition are set to calculate the surface temperature distribution through the hot-node network method[4][5]. Physics-based model requires the solution of three-dimensional heat transfer equation to get the distribution of surface radiation with high precision. It is quite time-consuming to solve a huge amount of heat balance equations, especially with a large number of surface patches. Empirical formula is the main method applied in the field of real time simulation. For aircraft flying for long periods of time or flying fast enough to generate aerodynamic heating, the stagnation temperature method is effective[3].

B. Reflection model

Various parametric BRDF models have been developed over the decades. These can be categorized into physically-based and empirical models. The former group includes microfacet-based models, such as the Torrance-Sparrow[6] and Cook-Torrance[7] models for specular surfaces, and the Oren-Nayar model[8] for diffuse surfaces. On the other hand, empirical models, such as the Phone[9], Blinn-Phong[10], and Lafortune models[11], use generic functions to express BRDFs. Compared with the mainstream models such as Phong model, Blinn-Phong model and Torrance-Sparrow model, Cook-Torrance model takes into account the details of the object such as surface roughness and variable structure[3].

C. Atmospheric transfer effect simulation

For atmospheric transfer effect simulation, the following kinds of radiative transfer calculation software are widely used: LOWTRAN series developed by the U.S. Air Force Geophysics Laboratory (AFGL), MODTRAN package improved from the LOWTRAN, FASCOD2 (Fast

Atmospheric Signature Code, Release2) developed by Philips Laboratory of the U.S. Hanscom Air Force and Distort package[1]. According to China's meteorological conditions, Tian et. al. used Lowtran 6 to calculate the average atmospheric transmittance of various parts of China, such as Northeast China, North China and East China, etc, and compiled the results into a look up table[12]. Wang et. al. obtained the fitting function under different conditions by polynomial fitting of the data results[13].

D. Infrared sensor model

As an important part of infrared imaging system, sensor modeling has brought many attentions over the past decade.. One of the sensor modeling tools called SYTHER (Synthesis of THERmal images) was developed by DASSAULT AVIATION. SYTHER's purpose was to generate realistic synthetic images of scenes made of landscapes and targets observed by a wide range of sensors in any IR waveband and in any environmental condition[14].

III. METHODOLOGY

The pipeline of our proposed infrared imaging simulation method is shown in Fig. 1. It can be seen that there are majorly four modules in the system, infrared modeling of small aerial target, dynamic background modeling, infrared sensor modeling, and target/background fusion.

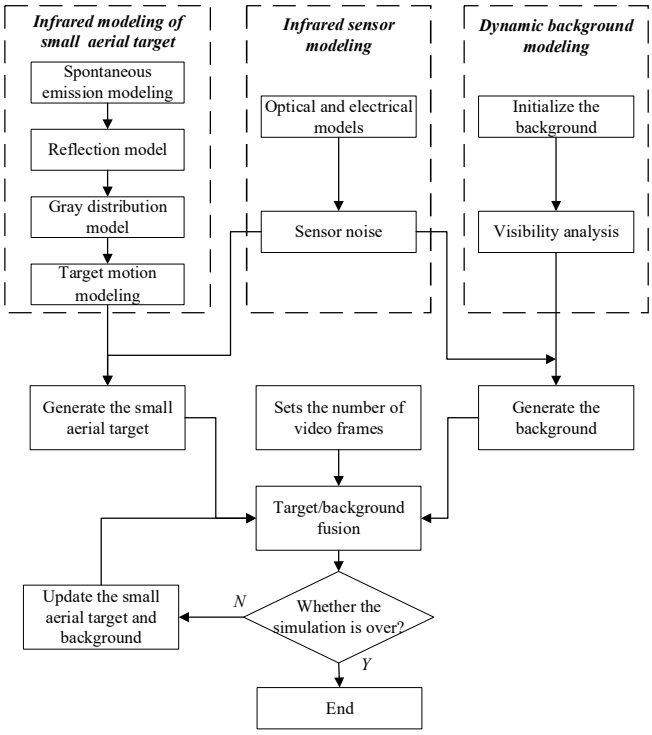

Fig. 1. Dynamic infrared image simulation process

A. Infrared modeling of small aerial target

1) Spontaneous emission modeling

The infrared radiation of the aircraft skin is a major component of aircraft self radiation, which comes from aerodynamic heating. When an aircraft flies at a high speed, the friction between its surface and air causes the surface temperature to rise sharply, thus generating infrared radiation. It is related to the surface temperature distribution and surface material emissivity.

Generally, the stagnation point temperature method, the heat balance equations method and the CFD flow field method are most commonly used in the calculation of skin temperature distribution. The stagnation point temperature method can intuitively represent the relationship between aircraft altitude, speed and temperature, which is very suitable for the aircraft.

Stagnation point temperature T_s can be calculated as[15],

$$T_s = T_\infty(1 + \gamma\frac{k-1}{2}M_a^2) \tag{1}$$

where T_∞ is the atmospheric temperature; M_a is the flight Mach number; and γ, k are constants, whose value can be set as 0.87 and 1.3.

The atmospheric temperature T_∞ at various altitude H is based on T_0 (the atmospheric temperature at sea level) .

$$T_\infty=\begin{cases} T_0\text{-}6.5H, & 0\le H\le 11\text{km} \\ T_0\text{-}71.5, & 11\le H\le 20\text{km} \\ T_0\text{-}71.5\text{+}H\text{-}20, & 20\le H\le 32\text{km} \end{cases} \tag{2}$$

According to Planck's formula, the infrared radiation intensity L_{self} of the aircraft skin can be calculated as,

$$L_{self} = \frac{\varepsilon}{\pi}\int_{\lambda_1}^{\lambda_2}\frac{2\pi hc^2}{\lambda^5}\frac{1}{e^{ch/\lambda kT_s}-1}\mathrm{d}\lambda \tag{3}$$

where ε is the surface emissivity, which is related to the material and temperature of the skin; T_s is the temperature of the skin surface. k is Boltzmann's constant; λ is the wavelength; h is Planck's constant; c is the speed of light.

2) Reflection model

The Cook-Torrance model is used to represent the specular reflection and diffusion reflection of the aircraft surface. The Cook-Torrance BRDF coefficient f_γ can be calculated as[7],

$$f_\gamma = k_d\frac{1}{\pi} + k_s\frac{F\,D\,G}{\pi\,(n\cdot v)(n\cdot l)} \tag{4}$$

where, k_d and k_s are the diffuse reflection and specular reflection coefficients respectively. $k_d + k_s = 1$. n is the normal vector of the surface; v is the direction of observation; and l is the incident direction vector.

F is the Fresnel reflection coefficient, which depends on the material properties of the surface:

$$F = f_0 + (1 - f_0)(1 - (v\cdot h))^5 \tag{5}$$

f_0 represents the base reflectivity of the plane. h is the half angular vector formed by vectors v and vectors l. In this paper, when calculating the reflection component, the small aerial target is assumed to be a facet whose normal vector is h.

D is the normal distribution function of the micro plane on the surface. The more uniform the normal direction distribution of the micro plane is, the smoother the plane will be. D determines the high light intensity of the surface, which is usually a Gaussian distribution:

$$D = \frac{1}{\pi m^2 cos^4\alpha}\,e^{-(\frac{tan\alpha}{m})^2} \tag{6}$$

where m is the roughness coefficient of the material on the surface, and α is the angle formed by the surface normal vector n and the half angle vector h.

$$cos\alpha = h\cdot n \tag{7}$$

G is the geometric attenuation factor. Due to the disorderly distribution of micro planes, the propagation of light between micro planes is blocked, so that the light can not be propagated out, resulting in attenuation of the reflection component:

$$G = \min\left(1, \frac{2(n\cdot h)(n\cdot v)}{h\cdot v}, \frac{2(n\cdot h)(n\cdot l)}{h\cdot l}\right) \quad (8)$$

According to the irradiance generated by the natural light source on the aircraft surface and the mathematical definition of BRDF, the reflected radiance L_{re} of the target in a specific direction can be calculated and obtained:

$$L_{re} = \int_{\lambda_1}^{\lambda_2} f_\gamma \cdot E_l \cdot (n \cdot l) d\lambda \quad (9)$$

In (9), f_γ is the BRDF coefficient of the surface, whose unit is $1\mathrm{sr}^{-1}$; E_l is the spectral irradiance of ambient lightis, whose unit is $w/(cm^2 * \mu m)$.

Eventually, the total infrared radiance L_{sum} of the skin is,

$$L_{sum} = L_{self} + L_{re} \quad (10)$$

3) Gray distribution model

Since this paper mainly studies the imaging of small aerial targets, in order to simplify the gray distribution, it can be assumed that the gray distribution of small aerial targets is a generalized Gaussian distribution[16].

The generalized Gaussian function has the following form:

$$G(x,y) = \frac{\rho_{\beta_x}\rho_{\beta_y}}{4\rho_{\alpha_x}\rho_{\alpha_y}\Gamma(\frac{1}{\rho_{\beta_x}})\Gamma(\frac{1}{\rho_{\beta_y}})} e^{-\left(\frac{|x-x_0|}{\rho_{\alpha_x}}\right)\rho_{\beta_x} - \left(\frac{|y-y_0|}{\rho_{\alpha_y}}\right)\rho_{\beta_y}} \quad (11)$$

where (x_0, y_0) is the center of the two-dimensional generalized Gaussian function; ρ_{α_x} and ρ_{β_x} are waveform control parameters and scale control parameters respectively on the x direction; similarly ρ_{α_y} and ρ_{β_y} are those on the y direction. When $\rho_{\beta_x} \to \infty$ and $\rho_{\beta_y} \to \infty$,two-dimensional generalized Gaussian function tends to be a uniform distribution, its domain is $\{(\mathrm{x},\mathrm{y})||x - x_0| < \rho_{\alpha_x}, |y - y_0| < \rho_{\alpha_y}\}$.It can be seen that the two-dimensional generalized Gaussian model can fit not only the peak signal, but also the flat top signal in practical application.

The signal orientation of the traditional two-dimensional generalized Gaussian function is fixed at the direction of the coordinate axis, which can not depict a small aerial target with irregular shape. So an angle factor is introduced to the two-dimensional generalized Gaussian function.

$$\begin{cases} x' = x_0 + (x - x_0)cos\rho_a - (y - y_0)sin\rho_a \\ y' = y_0 + (y - y_0)cos\rho_a - (x - x_0)sin\rho_a \end{cases} \quad (12)$$

where (x', y') is the new coordinate after the rotation of the point (x, y), and (x_0, y_0) is the rotation center of the angle. In this paper, the center of rotation is the same point as the center of two-dimensional generalized Gaussian function. ρ_a is the rotation angle, $\rho_a > 0$ for counterclockwise rotation.

4) Target motion modeling

Since this paper mainly studies the infrared simulation of small aerial targets, in this case , the aircraft can be simplified to be an ellipsoid. During the simulation process, the ellipsoid is projected from the 3D world coordinates to the 3D camera coordinates, and then to the 2D image coordinates system using the camera perspective model.

Given the simulation scenario, the kinematic models of the aircraft and the observer (infrared camera) can be set up accordingly. Or the simulation system can also take the predefined motion trajectories, which makes the system flexible for different applications. For example, for simulation of UAV sense and avoid, trajectories of two drones with potential collision risks can be set for testing.

B. Dynamic background modeling

Some studies simply adopted static background in infrared imaging simulation[2]. However, in airborne platform, due to the aircraft movement and vibration, and different points of view of the infrared camera, it would be more natural to simulate a dynamic background. In this paper, by setting the position and scale of any sky background image in the world coordinate system, and then analyzing the visibility using the perspective model of camera, we get the initial background image. Then by adding camera vibration, a dynamic background is obtained.

1) Initialize the background

Fig. 2 shows the position of the background image in the world coordinate system. The pixel point *P* in the background image is set as the anchor point to locate the image. The position of the background image is determined by modifying the position of point *P* in the world coordinate system. Then the scale of the background is initialized.

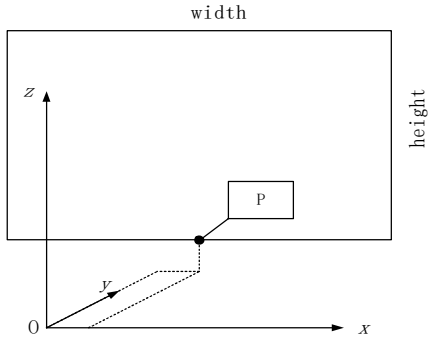

Fig. 2. Background image in the world coordinate system

2) Visibility analysis

In this paper, ray casting algorithm[3] is used to analyze the visibility of the background. The principle is shown in Fig. 3. If the light emitted from the camera position passing through the pixel position of the camera screen intersects the background, the pixel value of the intersection point is assigned to the corresponding camera screen point; If not, the corresponding screen point will be assigned a value of 0. By updating the value of each pixel of the camera screen, the image of the camera screen is finally obtained.

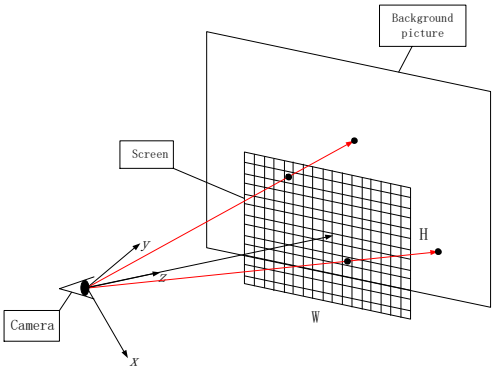

Fig. 3. Ray casting algorithm

C. Infrared sensor modeling

1) Optical and electrical models

According to the optical model of the infrared camera, the output voltage V_s of the sensor is :

$$V_s = R_v \cdot L_{sum} \cdot \frac{R^2 \cdot A_d}{f^2} \cdot \frac{\pi (D/2)^2}{R^2} \cdot \tau \cdot \text{opptrrans} \quad (13)$$

R_v is the sensitivity of the sensor; L_{sum} can be obtained by equation (10); R is the distance between the sensor and the aircraft; A_d is the effective area of the photosensitive element of the sensor, and f is the effective focal length of the optical system; D is the aperture of the optical system; τ is the transmittance of the atmosphere in the observed path; Opptrrans is the optical transmittance of the sensor.

To get the the transmittance τ of the atmosphere, software packages like Lowtran or Modtran are often used. Usage of these software are complicated.In order to simplify the process and integrate the computation of atmospheric transmittance into our simulation system, a fitted polynomial function in [13] is adopted to get the atmospheric transmittance simply.

After photoelectric conversion, the response voltage V_s is obtained, and then converted to the corresponding gray value G.

$$V_s = \begin{cases} V_L, & V_s < V_L \\ V_H, & V_s > V_H \\ V_s, & otherwise \end{cases} \quad (14)$$

$$G = G_{min} + \frac{(V_s - V_L)(G_{max} - G_{min})}{V_H - V_L} \quad (15)$$

where $G_{min} \sim G_{max}$ is the corresponding grayscale quantization range, and the upper limit and lower limit of the output voltage are V_H and V_L.

2) Sensor noise

Sensor noise is inevitable. Many types of sensor noise can be represented as Poisson noise, such as photoelectric conversion noise, signal circuit noise and transition noise. And thermal noise and temperature noise can be usually represented as Gaussian noise. Hence, in the proposed system, Possion noise and Gaussian noise are artificially added.

D. Target/background fusion

The gray value obtained by gray mapping is taken as the maximum value of small aerial target gray distribution. Then the small aerial target image patch can be generated according to the generalized Gaussian model. An image fusion process is needed to combine the small aerial target image patch and the background together.

Weighted average fusion and maximum or minimum fusion are commonly used in image fusion. However, both of these methods are based on the fusion of isolated pixels. None of these methods can achieve smooth transition on the boundary of the image overlapping area. The gradient field information of image can be used to fulfill smooth transition on the fusion edge. In this paper, we adopted Poisson fusion[17].

As shown in Fig. 4, in the Poisson fusion model, u is the fused part, V is the gradient field of u, and S is the image after fusion. The gradient field in Ω region is the same as V, while ∂ is its boundary, and the boundary pixel value is the same as the background pixel value. The pixel value in the Ω region is represented by f, and the pixel value outside the Ω region is represented by f^*.

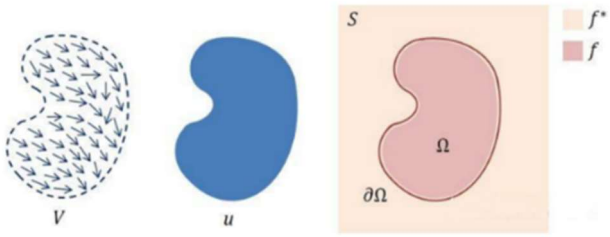

Fig. 4. Poisson fusion model

If we want to retain the texture information of the fused image and achieve a smooth transition without obvious processing traces at the edges, the optimization problem can be expressed as the following formula[2]:

$$\min_f \iint_\Omega \|\nabla f - V\|^2 = \min_f \iint_\Omega \|\nabla f - \nabla u\|^2, \text{ s.t.} f|_{\partial\Omega} = f^*|_{\partial\Omega} \quad (16)$$

In order to make the area of Ω in the fused image as close as possible to u, the gradient field V of u is used as the guide field of the solution equation. The Euler-Lagrange equation can be used to obtain the following equation:

$$\frac{\partial^2 f}{\partial x^2} + \frac{\partial^2 f}{\partial y^2} = \frac{\partial^2 u}{\partial x^2} + \frac{\partial^2 u}{\partial y^2} \quad (17)$$

The discrete formula of Laplace operator is:

$$\Delta u(i,j) = u(i+1,j) + u(i-1,j) + u(i,j+1) + u(i,j-1) - 4u(i,j) \quad (18)$$

Then the original Poisson equation becomes as follows:

$$f(i+1,j) + f(i-1,j) + f(i,j+1) + f(i,j-1) - 4f(i,j) = \Delta u(i,j) \quad (19)$$

Then we get:

$$f(i,j) = \frac{1}{4}(f(i+1,j) + f(i-1,j) + f(i,j+1) + f(i,j-1) - \Delta u(i,j)) \quad (20)$$

By solving Poisson's equations, the optimal pixel value in region Ω can be obtained.

IV. SIMULATION AND ANALYSIS

A. Simulation of spontaneous infrared radiation

Stagnation point temperature expression can intuitively show the relationship between skin spontaneous infrared radiation and aircraft velocity. Fig. 5 shows that when the aircraft is at an altitude of 20km, different flight speeds lead to different infrared radiation of the skin. It can be seen from Fig. 5 that the flight speed of the aircraft has almost no effect on infrared radiation at short-wave band. But at long-wave band, the faster the aircraft is, the stronger the infrared radiation will be.

Fig. 6 shows the infrared radiation of the aircraft skin at different flight altitudes when the flight speed is 1.2Ma. As can be seen, the general trend is that the altitude of the aircraft is negatively correlated with its spontaneous emission.

From the above observations, it can be found that most of the spontaneous infrared radiation energy of the aircraft is concentrated at the wavelength range of 8 to 12 μm. The result agrees with that in [18].

According to [3][18], the atmosphere is selective in the absorption of radiation. And the transmittance of the atmosphere is high in the band with weak absorption capacity. The wave band with higher atmospheric transmittance is called atmospheric window. In engineering, the infrared atmospheric window is usually divided into three bands: 1~3μm, 3~5 μm and 8~14μm. Considering the above factors, we choose to simulate the infrared radiation in the band of 8-12 μm.

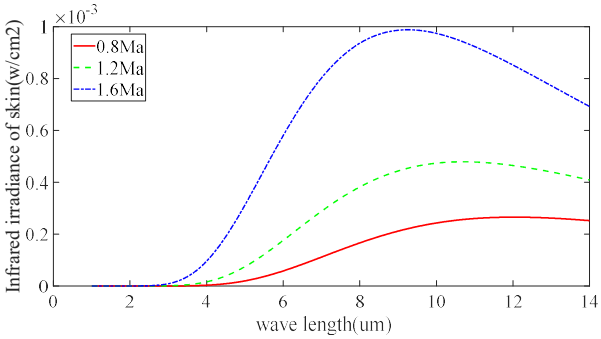

Fig. 5. Spontaneous emission of skin at different flight speeds

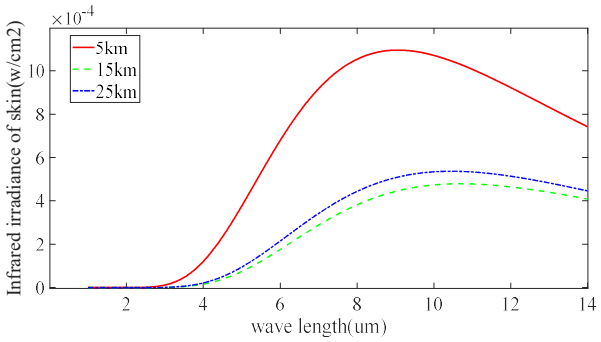

Fig. 6. Spontaneous emission of skin at different flight height

B. *Simulation of small aerial targets*

Using generalized Gaussian model, the small aerial target images with various gray distribution can be obtained. Fig. 7 shows the generated small aerial target images with different shapes.

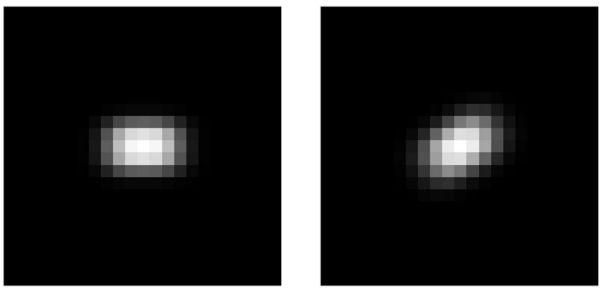

(a) (b)

Fig. 7. The generated small aerial target images. (a) Model parameters: $\rho_{\alpha_x} = 3, \rho_{\alpha_y} = 2, \rho_{\beta_x} = 3, \rho_{\beta_y} = 3, \rho_\alpha = 0$;(b) Model parameters: $\rho_{\alpha_x} = 3, \rho_{\alpha_y} = 2, \rho_{\beta_x} = 3, \rho_{\beta_y} = 3, \rho_\alpha = \pi/6$.

C. *Dynamic background simulation*

We select an infrared image of the sky, set the size and position of the background, and then set the position and attitude of the camera. Through visibility analysis, we can get the corresponding image. If the camera is set to the vibrational state, we can get the background simulation under the camera vibration condition, which is closer to the real situation. Fig. 8 shows a series of dynamic background simulation images.

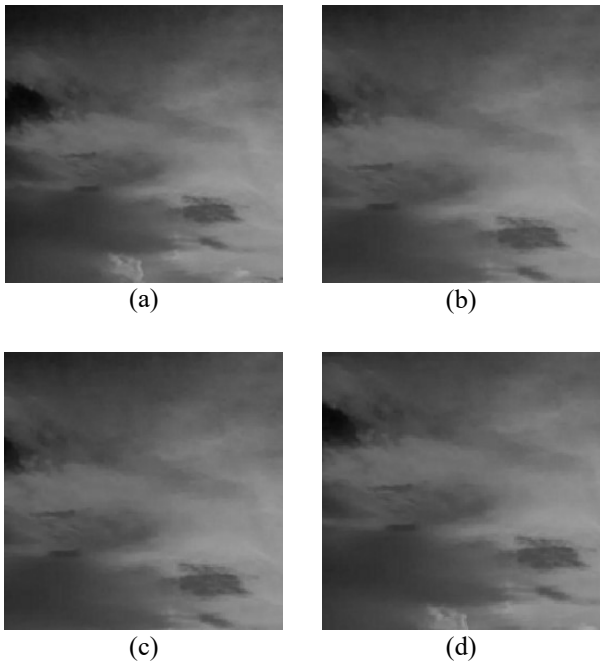

(a) (b)

(c) (d)

Fig. 8. Dynamic background images generated when camera is set to the vibrational mode. The camera is at position [0,0,8]. The camera shake amplitude is 0.3 degrees. Point P in the background is at [0,30,6]. The width and height of the background are 4km and 4km respectively.

D. *Dynamic infrared simulation sequence*

By setting the motion equation of the aircraft as well as the position and state of the camera, the infrared simulation sequence of the dynamic small aerial target under the sky background can be obtained.

Fig. 9 is a simulated sequence using a clear sky background. Notice that areas in red circles are the real target from an infrared video sequence. It can be seen that the simulated target is similar to the real one. Fig. 10 is the simulation result using a cloudy sky background. For both simulation, we assume that the kinematic model of the target is: $X(t) = 0.34t + 0.5 \times 0.01t^2$, $Y(t) = 0.34t + 4$, $Z(t) = 0.01t + 8$. All distance units are km.

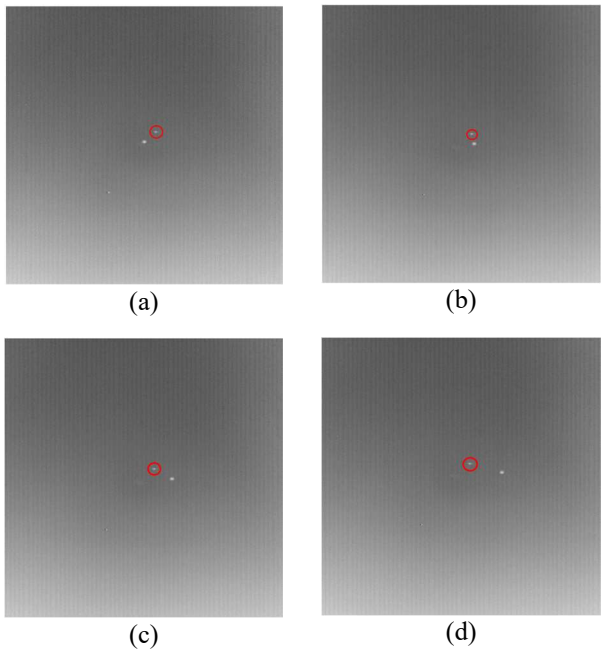

(a) (b)

(c) (d)

Fig. 9 Simulation results using a clear sky background.

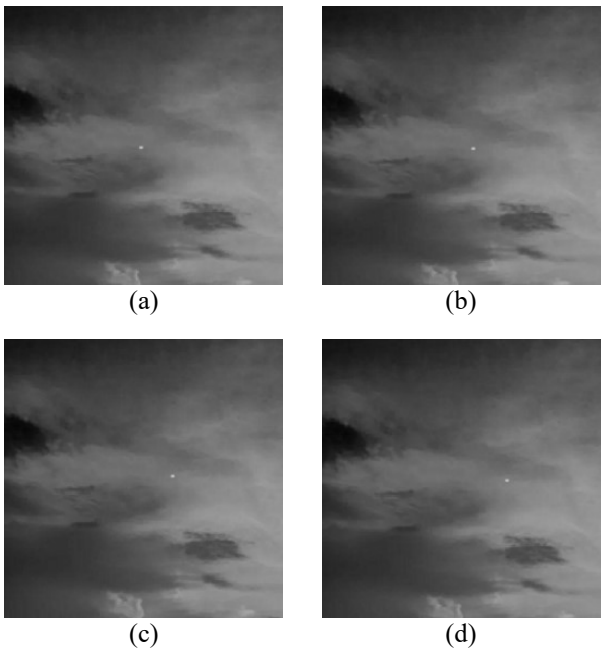

Fig. 10. Simulation results using a cloudy sky background.

The simulation is tested on a laptop with DDR4 8GB of running memory and an Intel(R) Core(TM) i7-7500U CPU(2.70GHz). The software used for simulation is Matlab 2019b. The average simulation time per frame is 0.28 s. The simulated image is in the resolution of 256 × 256. The proposed system runs in nearly real time.

V. CONCLUSION

In this paper, we propose an infrared imaging simulation system of small aerial targets. The infrared radiation model of the target, including spontaneous radiation model and reflection model, is studied. The generalized Gaussian model is used to simplify the gray distribution model of the target. Background is initialized using any infrared sky image and then adjusted the visibility by the camera perspective model. Then simulated target is fused with the simulated background using Poisson fusion for the generation of a more natural image. A dynamic simulation is fulfilled by assuming kinetics models of the target and the observer. So different encountering scenarios between the target and the observer can be simulated easily. Experiments show that the simulation results are very similar to the real infrared images.

For experimental result evaluation, ideally the simulated results should be compared to real infrared data. However, due to the limitation of experimental conditions, it would be challenging to generate all the true infrared data under various settings, especially for small aerial targets we studied. Hence, most existing studies either evaluate the simulation results by human observation, or simply compare the simulation with the real data under controlled environment. For example, Wang [3] took infrared images of a cup in their lab for system evaluation. It is a scenario which can be easily controlled. Our future work may involve the study of evaluation metrics.

In the process of simulation, the transmittance τ of atmospheric transmission is related to weather conditions. At present, τ is obtained by artificially specifying the weather conditions from the background image. One possible future direction is that weather conditions can be inferred from any given background image automatically using machine learning or deep learning algorithm. So the parameter τ can be decided automatically and the entire simulation process will need less user specification.

ACKNOWLEDGMENT

This work is supported by Aeronautical Science Foundation of China (No. 2018ZC53041).

REFERENCES

[1] N. Li, Z. Y. Su, Z. Cheng, and D. Han, A real-time aircraft infrared imaging simulation platform[J], Optik-International Journal for Light and Electron Optics, 124(17):2885-2893, 2013.

[2] L. Zhong, Forward modeling and simulation technology of infrared dim small targets under the complex background[D], Master Thesis, University of Electronic Science and Technology of China, 2016.

[3] X. Wang, Infrared Radiation Analysis and Imaging Simulation of Aerial Target[D], Ph.D dissertation, Shanghai Institute of Technical Physics Chinese Academy of Sciences, 2020.

[4] N. Li, Z. H. Lv, S. D. Wang, G. H. Gong and L. Ren, A real-time infrared radiation imaging simulation method of aircraft skin with aerodynamic heating effect[J], Infrared Physics & Technology 71: 533-541, 2015.

[5] T. Gonda, D.M. Less, D. Filbee, E. Polsen and T. Edwards, An explanation of vehicle-terrain interaction in IR synthetic scenes, Proc. SPIE 5075: 9–19, 2003.

[6] K. Torrance and E. Sparrow. Theory for off-specular reflection from roughened surfaces[J], Journal of the Optical Society of America, 57(9):1105–1114, 1967.

[7] R. Cook and K. Torrance. A reflectance model for computer graphics[J], ACM Transactions on Graphics, 1(1):7-24, 1982.

[8] M. Oren and S. Nayar, Diffuse reflectance from rough surfaces[C], In Proc. of IEEE Conference on Computer Vision and Pattern Recognition (CVPR), 1993.

[9] B. Phong, Illumination for computer generated pictures[J], Communications of the ACM, 18(6):311-317, 1975.

[10] J. Blinn, Models of light reflection for computer synthesized pictures[J], Computer graphics, 11(2):192-198, 1977.

[11] E. Lafortune, S. Foo, K. Torrance and D. Greenberg, Nonlinear approximation of reflectance functions[J], Computer Graphics and Interactive Techniques, 1997.

[12] L. H. Tian , L. W. Guo, Y. X. Yin, Handbook of the transmittance of infrared radiation in the atmosphere[M]. Ordnance Industry Press, Beijing, 1992.

[13] Y. F. Wang, J. X. Mao, Polynomial fitting calculation of atmospheric transmittance in 8 μ m~12 μ m spectral band with MATLAB[J], Infrared(Monthly), 29(1):15-19, 2008.

[14] Z. Liu, H. X. Mao, Y. H. Dai and J. L. Wu, A new infrared sensor model based on imaging system test parameter[C], Green Computing & Communications International Society for Optics and Photonics, 2013.

[15] K. F. Wu, Y. Zhou, J. Ma and J. Lin, Skin coating design of stealth aircraft based on infrared characteristic analysis[J], Materials Science Forum, 976:50-54, 2020.

[16] J. J. Zhao , Z. Y. Tang , J Yang and E. Q. Liu, Infrared small target detection using sparse representation[J], Journal of Systems Engineering and Electronics, 22(6):897-904, 2011.

[17] X. Jin, Q. Jiang, S. W. Yao, D. M. Zhou, R. C. Nie, et al. A survey of infrared and visual image fusion methods[J], Infrared Physics & Technology 85:478-501, 2017.

[18] W. Sun and B. Wang, Modeling and simulation of airplane infrared signature using fluent[C], Proceedings of the Conference on Control and its Applications (CT): 25-29, 2019.